Development of a Sensorless Control Method for a Self-Energizing Brake System Using Noncircular Gears

Heeram Park and Seibum B. Choi

***Abstract*— Electronic wedge brake (EWB) system, first introduced by Siemens VDO, is an efficient way to control a large brake clamping force electronically using a small electric motor. It is designed to amplify the clamping force of electromechanical brakes using a self-energizing effect. However, EWB is very sensitive to variations of system parametric errors, such as the friction coefficient variance during braking. The effect of parametric errors is highly amplified through the same self-energizing mechanism. A new type of EWB mechanism called an electronic noncircular gear brake is developed to avoid the potential problem due to the contamination of moving parts under very harsh operating conditions. Considering the sensitivity to parametric variation and the cost issue of clamping force measurement, a new sensorless adaptive control algorithm is developed, which functions without clamping force measurement. The robustness of the developed algorithm is verified through simulations and experiments.**

***Index Terms*— Adaptive control, electronic wedge brake (EWB), self-energizing, sensorless.**

I. Introduction

DUE TO the depletion of fossil fuels and current environmental regulations implemented to counter environmental pollution, vigorous research and development efforts are being made in the fields of electric vehicles and hybrid electric vehicles, both of which offer such advantages as low pollution and high fuel efficiency. Regenerative brake technology accounts for the largest portion of technologies designed to enhance the efficiency of such vehicles. Regenerative brake technology converts the kinetic energy of a vehicle, which would normally be lost as frictional heat generated between a brake disc and a pad upon braking, into electric energy, stores it in a battery, capacitor, or mechanical energy storage device, and uses it again upon operation. Depending on the energy recovered in this manner, the drivers' braking input and braking capabilities vary. Hence, a brake-by-wire technology is required. With this technology, the driver does not make physical contact with a mechanically connected braking device. Rather, braking capabilities are controlled by a hydraulic unit, or an electric actuator via an electric control device that receives the driver's intention of braking.

The brake-by-wire system offers other advantages aside from its use in regenerative brake technology: it reduces the braking distance owing to its rapid responsiveness and eliminates the need to use existing hydraulic systems. The latter can make it lightweight and secures design space, thereby allowing the use of anti-lock brake system, traction control system, and electronic safety program systems without additional hardware. Brake-by-wire systems can be divided into electrohydraulic brake (EHB), electromechanical brake (EMB), and electronic wedge brake (EWB) systems.

The EHB system controls braking capabilities through a hydraulic electronic control unit, by removing the vacuum booster from the existing brake system and receiving the drivers' braking input as an electric signal. However, this system entails the same issues as the existing hydraulic brake system, such as environmental pollution caused by brake fluid and difficulties related to maintenance and the power source.

The EMB system is free of all hydraulic systems found in existing brake systems and controls all braking capabilities with electronic devices, thereby easily affording optimal control of the braking capabilities and reducing vehicle stopping distance by 5% compared to the EHB system. However, it is accompanied by the disadvantage that it cannot be used in existing 12-V systems but rather in 42-V systems only, as it consumes a great deal of energy to obtain required braking capabilities.

The EWB system, developed by Siemens VDO, has the highest energy efficiency among brake-by-wire systems and can be used in existing 12-V systems, as it exploits self-energizing effect by the structural characteristics of a wedge-shaped member. Also, it can reduce vehicle stopping distance up to 15% compared to hydraulic brakes.

While the EWB system can greatly amplify the actuator's force through this self-energizing effect, it suffers the problem of amplification of error as well, which may undermine and deteriorate the systems' performance. The amplified gain of the EWB system is determined by the wedge angle and brake pad friction coefficient. Because the friction coefficient is not a constant value but fluctuates, it is difficult to control it with a simple proportional–integral–derivative-type controller. Hence, Hwang developed a control algorithm using sliding mode control, a nonlinear control technique reported in 2007 [7]. He also developed a method to estimate the friction coefficient, which greatly influences the systems' gain.

Manuscript received May 11, 2011; revised December 29, 2011; accepted May 8, 2012. Manuscript received in final form June 8, 2012. Date of publication August 20, 2012; date of current version June 14, 2013. This work was supported in part by the National Research Foundation of Korea funded by the Korea Government, under Grant 2012-0000991. Recommended by Associate Editor C. Bohn.

The authors are with the Department of Mechanical Engineering, Automotive Control Laboratory, Korea Advanced Institute of Science and Technology, Daejeon 305-701, Korea (e-mail: hrpark@kaist.ac.kr; sbchoi@kaist.ac.kr).

Color versions of one or more of the figures in this paper are available online at http://ieeexplore.ieee.org.

Digital Object Identifier 10.1109/TCST.2012.2204750

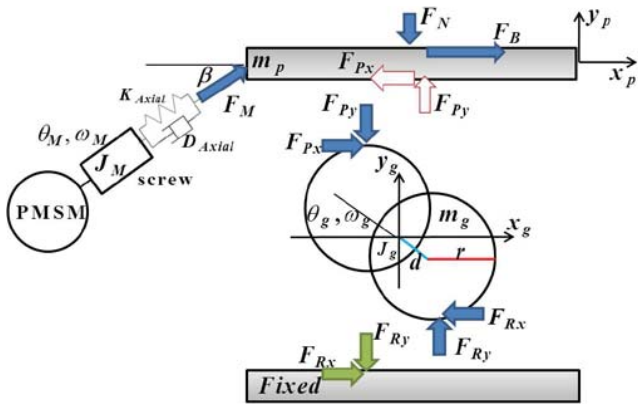

Fig. 1. Single-motor-electronic noncircular gear brake system.

In order to enhance the self-energizing effect in a EWB system, the friction between the wedge and caliper housing must be reduced. In general, friction is commonly reduced by using a roller between the wedge and caliper housing. However, if strong force is repeatedly applied to the roller, the roller will be worn out partially, thus undermining its effect. Kim developed a new type of brake system using oval-shaped gears in 2008 [8]. While this brake system exploits self-energizing effect as with the EWB system, various wedge angles can also be applied. Kim made the first prototype of a self-energizing brake using a noncircular gear. However, for the simplicity of machining, the gear was fabricated with two circular gears partially overlapping each other.

This paper investigates kinetics and dynamics of this fabricated brake system. A ball screw is used in order to reduce friction during actuation, and a permanent magnet synchronous motor (PMSM) is adopted to address the issue of durability. Caliper stiffness is measured to obtain an accurate model, and it is found that the stiffness is not a constant but rather varies in proportion to the caliper displacement. In this paper, a brake system model using a new actuator and reflecting nonlinearity of the caliper is implemented. Also, a controller is designed based on the implemented plant model, and an adaptive control algorithm is developed so that the model can adapt to parametric changes. Performance of the developed control algorithm is validated through simulations and experimental works.

II. Modeling

Fig. 1 illustrates the structure of the noncircular gear self-energizing brake system to which the PMSM is applied. Where, θ_M and ω_M represent the position and speed of the motor, K_{Cal} the stiffness of the caliper, K_{Axial} and D_{Axial} the stiffness and damping coefficient of the screw, and θ_g and ω_g the angular displacement and angular speed of the noncircular gear.

The following explains the operation of the self-energizing brake using the noncircular gear. The controller commands the motor using a 12-V battery power. The screw connected to the motor converts the rotary motion of the screw into linear motion of the screw nut. The link connected to the screw nut pushes the pad into the caliper housing with an angle β and force F_M. Due to F_M, reaction forces F_{Px} and F_{Py} in the parallel and normal directions are generated between the pad and the noncircular gear, as well as reaction forces F_{Rx} and F_{Ry} in the parallel and normal directions between the gear and the housing. Due to the force generated, the noncircular gear spins, and the pad in turn pushes down the disc due to the movement of the noncircular gear. Clamping force F_N is applied to the disc through the caliper with stiffness F_{Cal}, and braking friction force F_B is generated by the friction μ between the disc and the pad. F_B again pulls the pad and amplifies the clamping force, thus providing self-energizing effect.

A. PMSM Modeling

The modeling of the PMSM uses Clarke and Park transform. Clarke and Park transform is a method commonly used to easily model, analyze, and control an alternating current system, and it converts coordinates, such as voltage, current, and magnetic flux into a more easily used format [9]. Clarke transform converts three-phase vectors into two-phase stator orthogonal coordinates. The formula for conversion of Clarke transform is shown in

$$\begin{bmatrix} f_\alpha \\ f_\beta \end{bmatrix} = \begin{bmatrix} 1 & 0 & 0 \\ 0 & \frac{1}{\sqrt{3}} & \frac{-1}{\sqrt{3}} \end{bmatrix} \begin{bmatrix} f_a \\ f_b \\ f_c \end{bmatrix}. \tag{1}$$

Park transform converts two-phase stator orthogonal coordinates into a two-phase $d-q$ axis, which is fixed to the rotor during rotation. Here, the d axis is in the same axis as the rotor flux. The formula for conversion of Park transform is shown in

$$\begin{bmatrix} f_\alpha \\ f_\beta \end{bmatrix} = \begin{bmatrix} \cos\theta & \sin\theta \\ -\sin\theta & \cos\theta \end{bmatrix} \begin{bmatrix} f_\alpha \\ f_\beta \end{bmatrix} \tag{2}$$

where θ is a rotational angle of the rotor.

Equations (3) and (4) are expressions of PMSMs voltage equations with $d-q$ coordinates

$$v_d = R_M i_d + \frac{d}{dt}\psi_d - \omega_s \psi_q \tag{3}$$

$$v_q = R_M i_q + \frac{d}{dt}\psi_q + \omega_s \psi_d$$

$$\psi_q = L_q i_q, \quad \psi_d = L_d i_d + \psi_{af} \tag{4}$$

where, v_d, v_q represent voltages, i_d, i_q currents of each axis, L_d, L_q the inductance of each axis, ψ_d, ψ_q flux linkage of each axis, ω_s the synchronizing velocity, R_M stator resistance, and ψ_{af} flux linkage by the rotor.

The motor's electric torque is shown in

$$T_M = \frac{2}{3} n_p \left[\psi_{af} i_q + \left(L_d - L_q\right) i_d i_q\right]. \tag{5}$$

Also, the motor equation of motion is shown in

$$T_M = T_L + J_M \dot{\omega}_M \tag{6}$$

where, n_p represents the number of pole pairs, ψ_{af} the flux linkage by the rotor magnet, J_M the angular moment of inertia, and ω_M the rotor's speed. The rotor's speed and synchronizing velocity are related to

$$\omega_s = n_p \omega_M. \tag{7}$$

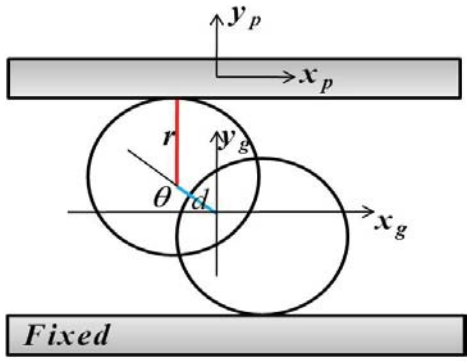

Fig. 2. Diagram of noncircular gear and pad.

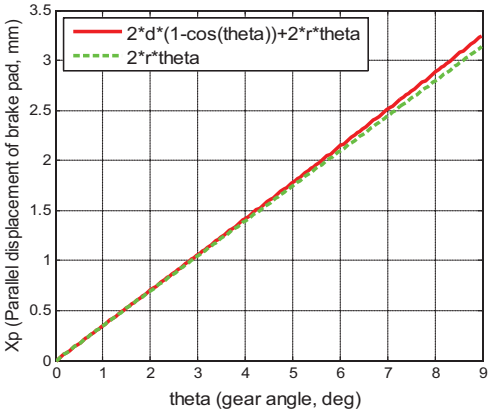

Fig. 3. Parallel direction displacement of noncircular gear angle and pad.

In order to generate maximum torque, PMSM is controlled such that the magnetic flux component current i_d becomes 0 [9]. Hence, the following relations are established:

$$\psi_d = \psi_{af} \tag{8}$$

$$T_M = \frac{2}{3} n_p \psi_{af} i_q = K_t i_M$$

$$K_t = \frac{2}{3} n_p \psi_{af}, \qquad i_M = i_q \tag{9}$$

$$L_M \dot{i}_M = -R_M i_M - K_e \omega_M + u_M$$

$$L_M = L_q, \qquad K_e = n_p \psi_{af}, \qquad u_M = v_q. \tag{10}$$

B. Noncircular Gear and Pad Modeling

Fig. 2 represents the movements of the gear and pad on a 2-D plane.

Where, x_p and y_p represent the pad's displacement in the parallel and normal directions, x_g and y_g the gear's displacement in the parallel and normal directions, θ_g the gear's angular displacement, r the diameter of the noncircular gear, and d half of the distance of the center between two circles of the noncircular gear. Equation (11) shows the relation between the pad's displacement in the parallel and normal directions, and the noncircular gear's angular displacement

$$\begin{aligned} x_g &= d(1 - \cos\theta_g) + r\theta_g \\ y_g &= d \sin\theta_g \\ x_p &= 2x_g \\ y_p &= 2y_g. \end{aligned} \tag{11}$$

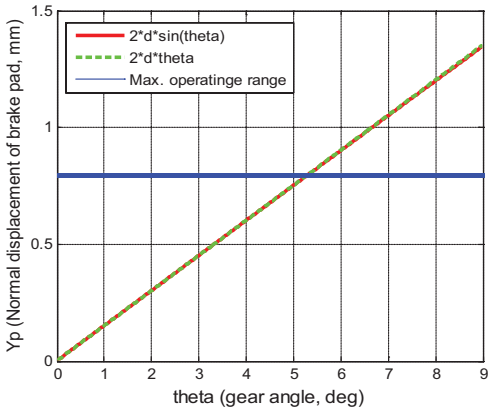

Fig. 4. Normal direction displacement of noncircular gear angle and pad.

TABLE I
ERROR OF APPROXIMATION

	Maximum error	Error(%)
Parallel direction	37.22 μm	1.96
Normal direction	1.15 μm	0.14

TABLE II
ERROR OF APPROXIMATION

	Maximum error	Error(%)
Clamping force F_N	117.32 N	3.06

Figs. 3 and 4 illustrate the relations between parallel and normal direction displacement of the pad and displacement of the gear angle. The gear works around 0 degree, and $\sin\theta_g$ and $\cos\theta_g$ can be approximated as θ_g and 1, respectively. The straight line in Figs. 3 and 4 is for (11), while the dotted line represents approximated values. As Table I shows the difference between the actual displacement and approximated values, is negligible compared to other modeling errors.

Equation (11) can be expressed with approximate values, as follows:

$$x_g = r\theta_g, \qquad y_g = d\theta_g, \qquad x_p = 2x_g, \qquad y_p = 2y_g. \tag{12}$$

Equations (13) and (14) represent the pad's motion in parallel and normal directions

$$m_p \ddot{x}_p = F_M \cos\beta + F_b - F_{Px} \quad F_b = \mu F_N \tag{13}$$

$$m_p \ddot{y}_p = F_M \sin\beta - F_N + F_{Py} \tag{14}$$

where m_p denotes the pad's mass and μ the friction coefficient between the pad and the brake disc.

Fig. 5 shows data of the clamping force F_N measured by using a load cell along with an approximated one as a function of pad normal displacement. Table II shows the maximum error between the measured clamping force and approximated one.

From the data measured, it is found that the caliper stiffness is not a constant but rather is a parameter dependent on the caliper displacement. The clamping force is expressed with

$$\begin{aligned} F_N &= K_{\text{Cal}} y_p \\ K_{\text{Cal}} &= K'_{\text{Cal}} y_p \\ F_N &= K'_{\text{Cal}} y_p^2. \end{aligned} \tag{15}$$

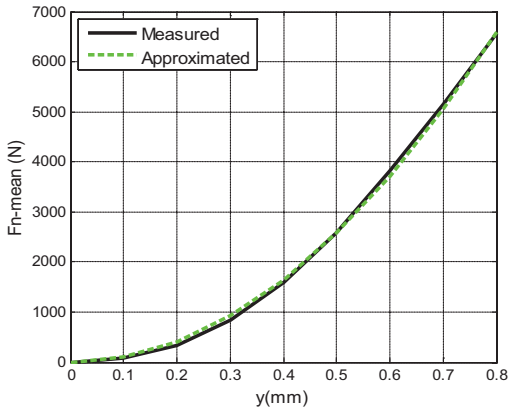

Fig. 5. Clamping force and caliper displacement.

Input force F_M delivered from the motor is defined as

$$F_M = -K_{\text{Axial}}\left(\frac{x_p}{\cos\beta} - \frac{L}{2\pi}\theta_M\right) - D_{\text{Axial}}\left(\frac{\dot{x}_p}{\cos\beta} - \frac{L}{2\pi}\omega_M\right) \tag{16}$$

$$2\pi\eta T_L = LF_M \tag{17}$$

where K_{Axial} denotes axial stiffness, D_{Axial} viscous damping, L screw lead, and η screw efficiency, respectively.

Equation (18) represents the gear's equation of motion in the parallel direction, while (19) provides the gear's equation of motion in the normal direction. Assuming $r + d\sin\theta_g \approx r$ and $d\cos\theta_g \approx d$, gear rotation is described as

$$m_g\ddot{x}_g = F_{Px} - F_{Rx} \tag{18}$$

$$m_g\ddot{y}_g = -F_{Ry} + F_{Py} \tag{19}$$

$$J_g\ddot{\theta}_g = r\left(F_{Rx} + F_{Px}\right) - d\left(F_{Ry} + F_{Py}\right) \tag{20}$$

where F_{Rx} and F_{Ry} represent the reaction force in the parallel and normal directions between the gear and the fixed caliper house, F_{Px} and F_{Py} the reaction force in the parallel and normal direction between the gear and the pad, r the diameter of one circle of the noncircular gear, and d half of the distance of the center between two circles of the noncircular gear.

Equation (21) is obtained by substituting (20) into (18) and (19)

$$J_g\ddot{\theta}_g = r\left(2F_{Px} - m_g\ddot{x}_g\right) - d\left(2F_{Py} - m_g\ddot{y}_g\right). \tag{21}$$

When (13) and (14) are substituted into (21)

$$\begin{aligned} J_g\ddot{\theta}_g &= 2rF_M\cos\beta + 2r\mu F_N - 2rm_p\ddot{x}_p - m_gr\ddot{x}_g \\ &\quad + 2dF_M\sin\beta - 2dF_N - 2dm_p\ddot{y}_p - dm_g\ddot{y}_g \\ M\ddot{\theta}_g &= (\cos\beta + \tan\alpha\sin\beta)F_M - (\tan\alpha - \mu)F_N \\ M &= \frac{J_g + \left(r^2 + d^2\right)\left(4m_p + m_g\right)}{2r} \\ \tan\alpha &= \frac{d}{r} \\ F_M &= -K_{\text{Axial}}\left(\frac{2r}{\cos\beta}\theta_g - \frac{L}{2\pi}\theta_M\right) \\ &\quad - D_{\text{Axial}}\left(\frac{2r}{\cos\beta}\omega_g - \frac{L}{2\pi}\omega_M\right)F_N = K_{\text{Cal}}^{'}\left(2d\theta_g\right)^2. \end{aligned} \tag{22}$$

Expressing the entire system in state space

$$x = \left[\theta_g\ \omega_g\ \theta_M\ \omega_M\ i_M\right]^T$$

$$y = H(x) = K_{\text{Cal}}^{'}\left(2d\theta_g\right)^2 = 4d^2K_{\text{Cal}}^{'}\theta_g^2$$

$$\dot{x} = \begin{bmatrix} 0 & 1 & 0 & 0 & 0 \\ -D_1 - D_2\theta_g & -D_3 & D_4 & D_5 & 0 \\ 0 & 0 & 0 & 1 & 0 \\ E_1 & E_2 & -E_3 & -E_4 & E_5 \\ 0 & 0 & 0 & -F_1 & -F_2 \end{bmatrix} x + \begin{bmatrix} 0 \\ 0 \\ 0 \\ 0 \\ F_3 \end{bmatrix} u_M$$

where

$$D_1 = \frac{K_{\text{Axial}}(\cos\beta + \tan\alpha\sin\beta)(2r)}{M\cos\beta}$$

$$D_2 = \frac{K_{\text{Cal}}^{'}(\tan\alpha - \mu)(2d)^2}{M}$$

$$D_3 = \frac{D_{\text{Axial}}(\cos\beta + \tan\alpha\sin\beta)(2r)}{M\cos\beta}$$

$$D_4 = \frac{K_{\text{Axial}}(\cos\beta + \tan\alpha\sin\beta)L}{M2\pi}$$

$$D_5 = \frac{D_{\text{Axial}}(\cos\beta + \tan\alpha\sin\beta)L}{M2\pi}$$

$$E_1 = \frac{K_{\text{Axial}}(2r)L}{J_M2\pi\eta\cos\beta},\quad E_2 = \frac{D_{\text{Axial}}(2r)L}{J_M2\pi\eta\cos\beta},\quad E_3 = \frac{K_{\text{Axial}}L^2}{J_M4\pi^2\eta}$$

$$E_4 = \frac{D_{\text{Axial}}L^2}{J_M4\pi^2\eta},\qquad E_5 = \frac{K_t}{J_M}$$

$$F_1 = \frac{K_e}{L_M},\qquad F_2 = \frac{R_M}{L_M},\qquad F_3 = \frac{1}{L_M}. \tag{23}$$

C. Self-Energizing Effect

Equation (24) is the relation of input force F_M and output force F_N at the steady state

$$F_N = \frac{(\cos\beta + \tan\alpha\sin\beta)}{(\tan\alpha - \mu)}F_M. \tag{24}$$

In the case of EWB, F_M is amplified depending on the relative magnitude of $\tan\alpha$ and the brake pad friction coefficient $\mu\cdot\mu$ can be change due to the brake fade. Since the systems' gain varies greatly depending on the value of μ, it is necessary to develop an algorithm that estimates the value so as to ensure accurate brake torque control. In this paper, the variation range of μ is from 0.2 to 0.6.

III. Controller Design

A. Singular Perturbational Model Reduction in the Frequency Domain

According to the model defined in the previous section, the ENGB systems' order is fifth, while its control relative order is fourth, indicating that it is a high-order system. When a controller is designed for and applied to a high-order system such as this one, a high-order derivation term is inevitably involved. An high-order derivation term is very difficult to use actual since the sensor's noise is greatly amplified. Therefore, the systems' order needs to be reduced.

In this paper, model-order reduction is performed by using the singular perturbational method [25]. The greatest advantage of this technique lies in its simplicity. The state space

representation of the noncircular gear brake system delineated in the previous section can be arranged as follows. For the simplicity of calculation, the caliper stiffness is linearized as the value at a specific position θ_g^* within the brake operating range

$$\dot{x} = Ax + Bu_M, \quad y = Cx, \quad x = \begin{bmatrix} \theta_M & \omega_M & \theta_g & \omega_g & i_M \end{bmatrix}$$
$$A = \begin{bmatrix} 0 & 1 & 0 & 0 & 0 \\ -E_3 & -E_4 & E_1 & E_2 & E_5 \\ 0 & 0 & 0 & 1 & 0 \\ D_4 & D_5 & -D_{12} & -D_3 & 0 \\ 0 & -F_1 & 0 & 0 & -F_2 \end{bmatrix}, \quad B = \begin{bmatrix} 0 \\ 0 \\ 0 \\ 0 \\ F_3 \end{bmatrix}$$
$$C = \begin{bmatrix} 0 & 0 & h & 0 & 0 \end{bmatrix}$$
$$D_{12} = \frac{K_{\text{Axial}}\,(1+\tan\alpha\,\tan\beta)\,(2r)+K_{\text{Cal}}^*\,(\tan\alpha-\mu)\,(2d)}{M} \times \left(K_{\text{Cal}}^* = K_{\text{Cal}} 2d\theta_g^*\right). \tag{25}$$

The system can be partitioned into two parts as follows:

$$A = \begin{bmatrix} A_{11} & A_{12} \\ A_{21} & A_{22} \end{bmatrix}, \quad B = \begin{bmatrix} B_1 \\ B_2 \end{bmatrix}, \quad C = \begin{bmatrix} C_1 & C_2 \end{bmatrix}$$
$$A_{11} = \begin{bmatrix} 0 & 1 \\ -E_3 & -E_4 \end{bmatrix}, \quad A_{12} = \begin{bmatrix} 0 & 0 & 0 \\ E_1 & E_2 & E_5 \end{bmatrix}$$
$$A_{21} = \begin{bmatrix} 0 & 0 \\ D_4 & D_5 \\ 0 & -F_1 \end{bmatrix}, \quad A_{22} = \begin{bmatrix} 0 & 1 & 0 \\ -D_{12} & -D_3 & 0 \\ 0 & 0 & -F_2 \end{bmatrix}$$
$$B_1 = \begin{bmatrix} 0 \\ 0 \end{bmatrix}, \; B_2 = \begin{bmatrix} 0 \\ 0 \\ F_3 \end{bmatrix}, \; C_1 = \begin{bmatrix} 0 & 0 \end{bmatrix}, \; C_2 = \begin{bmatrix} h & 0 & 0 \end{bmatrix}. \tag{26}$$

The transfer function can then be described as

$$G(s) = \begin{bmatrix} C_1 & C_2 \end{bmatrix} \begin{pmatrix} sI - A_{11} & -A_{12} \\ -A_{21} & sI - A_{22} \end{pmatrix}^{-1} \begin{bmatrix} B_1 \\ B_2 \end{bmatrix}. \tag{27}$$

Above transfer function can be expressed as follows by using inverse of partitioned matrices lemma [25]

$$G(s) = G_1(s) + G_2(s)$$

where

$$\begin{aligned} G_1(s) &= \bar{C}(s)\left[sI - \bar{A}(s)\right]^{-1}\bar{B}(s) \\ \bar{A}(s) &= A_{11} + A_{12}(sI - A_{22})^{-1}A_{21} \\ \bar{B}(s) &= B_1 + A_{12}(sI - A_{22})^{-1}B_2 \\ \bar{C}(s) &= C_1 + C_2(sI - A_{22})^{-1}A_{21} \\ G_2(s) &= LC_2(sI - A_{22})^{-1}B_2. \end{aligned} \tag{28}$$

If subsystem $G_2(s)$ is stable and is not dominant in the neighborhood of the frequency of interest, $s = \sigma_0$, the system $G(s) = G_1(s) + G_2(s)$ can be approximated as a reduced-order representation $G_1(s) = \bar{C}(s)[sI - \bar{A}(s)]^{-1}\bar{B}(s)$. The characteristic equation and Eigen value of the subsystem $S(A_{22}, B_2, C_2)$ are given as follows:

$$\left(s^2 + D_3 s + D_{12}\right)(s + F_2) = 0$$
$$\lambda_{1,2} = -790.04 \pm 10500.66i, \quad \lambda_{1,2} = -6285.71. \tag{29}$$

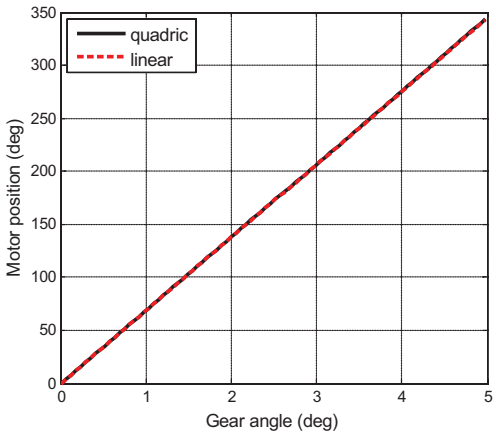

Fig. 6. Relationship between motor position and gear angle.

Therefore, the above subsystem is stable. Since the brake operates at a low-frequency range of 10 Hz or below, the subsystem represented by (29) can be neglected. The zeroth-order singular perturbational result at $s = 0$ is as follows:

$$\bar{A}(0) = \begin{bmatrix} 0 & 1 \\ -E_3 + \frac{D_4 E_1}{D_{12}} & -E_4 + \frac{D_5 E_1}{D_{12}} - \frac{E_5 F_1}{F_2} \end{bmatrix}$$
$$\bar{B}(0) = \begin{bmatrix} 0 \\ \frac{E_5 F_3}{F_2} \end{bmatrix}, \quad \bar{C}(s) = \begin{bmatrix} \frac{D_4 h}{D_{12}} & \frac{D_5 h}{D_{12}} \end{bmatrix}. \tag{30}$$

If the system is solved and rearranged using $\bar{A}(0)$

$$\begin{aligned} \bar{A}_{21} &= -E_3 + \frac{D_4 E_1}{D_{12}} = \frac{-\frac{K_{\text{Cal}}^*(\tan\alpha-\mu)\cos\beta(2d)L^2}{J_M 4\pi^2\eta(\cos\beta+\tan\alpha\sin\beta)(2r)}}{\left[1 + \frac{K_{\text{Cal}}^*(\tan\alpha-\mu)\cos\beta(2d)}{K_{\text{Axial}}(\cos\beta+\tan\alpha\sin\beta)(2r)}\right]} \\ &\approx -\frac{K_{\text{Cal}}^*(\tan\alpha-\mu)\cos\beta(2d)L^2}{J_M 4\pi^2\eta(\cos\beta+\tan\alpha\sin\beta)(2r)} \\ &= -\frac{K_{\text{Cal}}(\tan\alpha-\mu)\cos\beta(2d)^2 L^2}{J_M 4\pi^2\eta(\cos\beta+\tan\alpha\sin\beta)(2r)}\theta_g \\ &\quad \left(1 + \frac{K_{\text{Cal}}^*(\tan\alpha-\mu)\cos\beta(2d)}{K_{\text{Axial}}(\cos\beta+\tan\alpha\sin\beta)(2r)} = 1.002\right) \end{aligned} \tag{31}$$

$$\begin{aligned} \bar{A}_{22} &= -E_4 + \frac{D_5 E_1}{D_{12}} - \frac{E_5 F_1}{F_2} = -\frac{D_{\text{Axial}} L^2}{J_M 4\pi^2\eta} \\ &\quad + \frac{D_{\text{Axial}} L^2}{J_M 4\pi^2\eta\left[1 + \frac{K_{\text{Cal}}^*(\tan\alpha-\mu)\cos\beta(2d)}{K_{\text{Axial}}(\cos\beta+\tan\alpha\sin\beta)(2r)}\right]} - \frac{K_t K_e}{J_M R_M} \\ &\approx -\frac{K_t K_e}{J_M R_M}. \end{aligned} \tag{32}$$

When $s = 0$ in (25), θ_g is related to θ_M as follows:

$$\theta_g(0) = \left(\frac{2\pi\,(2r)}{L} + \frac{K_{\text{Cal}}^*(\tan\alpha-\mu)\,2\pi\,\cos\beta\,(2d)}{K_{\text{Axial}}\,(\cos\beta+\tan\alpha\sin\beta)\,L}\right)^{-1}\theta_M(0). \tag{33}$$

When (33) undergoes inverse Laplace transform, and K_{Cal}^* is expressed as a function of θ_g

$$\theta_M = \frac{2\pi\,(2r)}{L\cos\beta}\theta_g + \frac{K_{\text{Cal}}(\tan\alpha-\mu)\,2\pi\,\cos\beta\,(2d)^2}{K_{\text{Axial}}\,(\cos\beta+\tan\alpha\sin\beta)\cos\beta L}\theta_g^2. \tag{34}$$

Fig. 6 is the graphical illustration of (34).

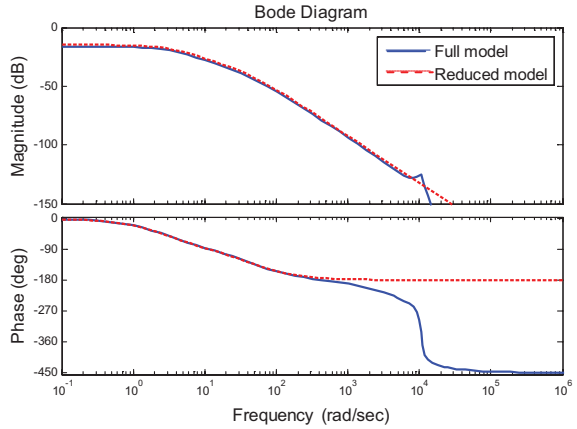

Fig. 7. Full and reduced model transfer functions.

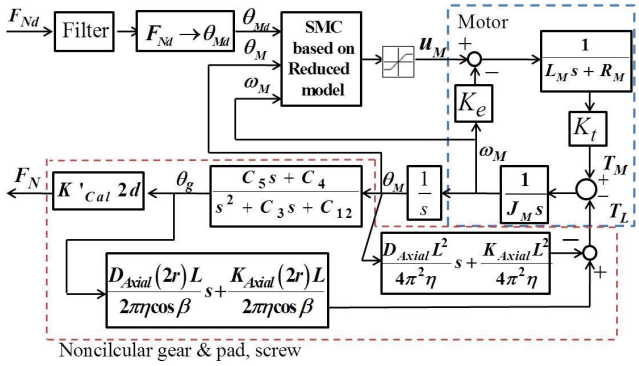

Fig. 8. Block diagram of the electronic noncircular gear brake control system.

Since the nonlinear effect due to θ_g^2 is negligible (34) can be approximated as follows:

$$\theta_g = \frac{L\cos\beta}{2\pi\ (2r)}\theta_M. \tag{35}$$

Equations for each element of $\bar{B}\ (0)$ and $\bar{C}\ (0)$ can be solved and rearranged as follows:

$$\bar{B}\ (0) = \begin{bmatrix} 0 \\ \frac{E_5 F_3}{F_2} \end{bmatrix} = \begin{bmatrix} 0 \\ \frac{K_e}{J_M R_M} \end{bmatrix}$$

$$\bar{C}\ (0) = \begin{bmatrix} \frac{K^*_{\mathrm{Cal}}(2d)L\cos\beta}{2\pi\ (2r)} & \frac{\frac{D_{\mathrm{Axial}}K^*_{\mathrm{Cal}}\cos\beta L(2d)}{K_{\mathrm{Axial}}2\pi\ (2r)}}{1+\frac{K^*_{\mathrm{Cal}}(\tan\alpha-\mu)(2d)}{K_{\mathrm{Axial}}(1+\tan\alpha\tan\beta)(2r)}} \approx 0 \end{bmatrix}. \tag{36}$$

In this paper, it is assumed that the screw is very stiff and D_{Axial} is negligible.

Finally, K^*_{Cal} is expressed as a function of θ_g, and the system is rearranged with respect to θ_M and ω_M using (36). The state space representation of the reduced model is as follows:

$$x_s = \begin{bmatrix} \theta_M\ \omega_M \end{bmatrix}^T, \qquad \dot{x}_s = \bar{A}\ (0)\, x_s + \bar{B}\ (0)\, u_M$$

$$y = \bar{C}\ (0)\, x_s$$

$$\bar{A}\ (0) = \begin{bmatrix} 0 & 1 \\ -\frac{K'_{\mathrm{Cal}}(\tan\alpha-\mu)\cos^2\beta(2d)^2L^3}{J_M 8\pi^3\eta(\cos\beta+\tan\alpha\sin\beta)(2r)^2}\theta_M & -\frac{K_t K_e}{J_M R_M} \end{bmatrix}$$

$$\bar{B}\ (0) = \begin{bmatrix} 0 \\ \frac{K_e}{J_M R_M} \end{bmatrix}, \quad \bar{C}\ (0) = \begin{bmatrix} \frac{K'_{\mathrm{Cal}}L^2\cos^2\beta(2d)^2}{4\pi^2(2r)^2} & 0 \end{bmatrix}. \tag{37}$$

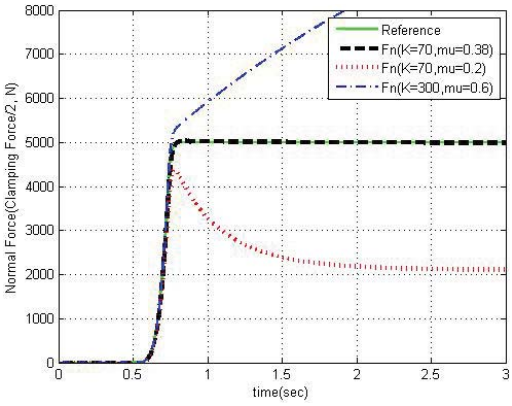

Fig. 9. Control response for various friction coefficients.

Fig. 7 compares the full model with the reduced model in frequency domain. It is confirmed that within the operating range of the brake (10 Hz = 62.8 rad/s), the full model and reduced model almost overlap. Therefore, the system can be expressed and controlled using the reduced model.

B. Model-Based Controller

A model-based controller is designed similar to sliding control design method. Tracking error ε and a variable s are defined as follows:

$$\varepsilon = y - y_d = \theta_M - \theta_{Md} \tag{38}$$

$$s = \left(\frac{d}{dt} + \lambda\right)\varepsilon = \dot{\varepsilon} + \lambda\varepsilon \tag{39}$$

where λ is a constant greater than 0. The control law is defined as follows for a positive constant K so that s converges to 0

$$\dot{s} = -Ks. \tag{40}$$

Differentiating (39)

$$\dot{s} = \ddot{\varepsilon} + \lambda\dot{\varepsilon} = \dot{\omega}_M - \dot{\omega}_{Md} + \lambda\left(\omega_M - \omega_{Md}\right). \tag{41}$$

Substituting (37) into (41)

$$\dot{s} = -p_1\theta_M^2 - p_2\omega_M + qu_M - \dot{\omega}_{Md} + \lambda\left(\omega_M - \omega_{Md}\right)$$

$$p_1 = \frac{K'_{\mathrm{Cal}}\left(\tan\alpha - \mu\right)\cos^2\beta\,(2d)^2\,L^3}{J_M 8\pi^3\eta\left(\cos\beta + \tan\alpha\sin\beta\right)(2r)^2}$$

$$p_2 = \frac{K_t K_e}{J_M R_M}, \qquad q = \frac{K_e}{J_M R_M}. \tag{42}$$

From (40) and (42), control input u_M is obtained as follows:

$$u_M = q^{-1}\Big[p_1\theta_M^2 + p_2\omega_M + \dot{\omega}_{Md} - (\lambda + K)\left(\omega_M - \omega_{Md}\right) - \lambda K\left(\theta_M - \theta_{Md}\right)\Big]. \tag{43}$$

Fig. 8 describes the entire control system. Figs. 9 and 10 show the simulation results of the reduced model-based controller using MATLAB Simulink. The straight line denotes reference clamping force, the bold dotted line reactions when the actual friction coefficient μ_P and modeled value μ_M are identical, and the dashed dot lines and thin straight lines reactions when μ_P is at its maximum and minimum.

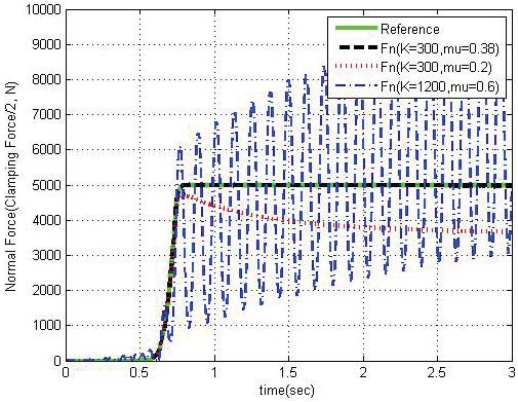

Fig. 10. High gain control response with measurement noise for various friction coefficients.

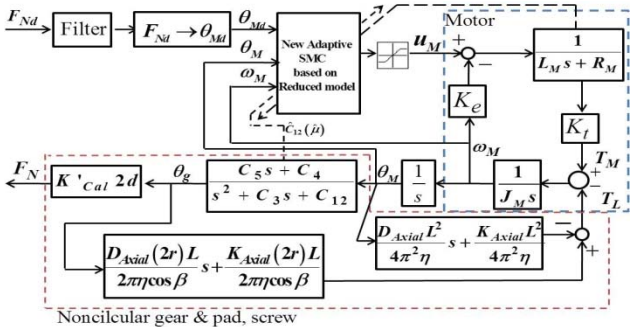

Fig. 11. Block diagram of the electronic noncircular gear brake control system.

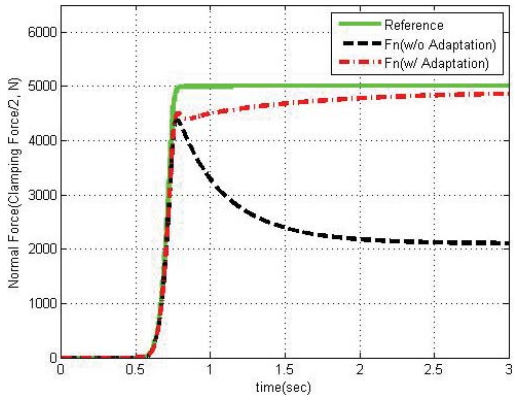

Fig. 12. Adaptive control with $\mu_{\text{Plant}} = 0.2$.

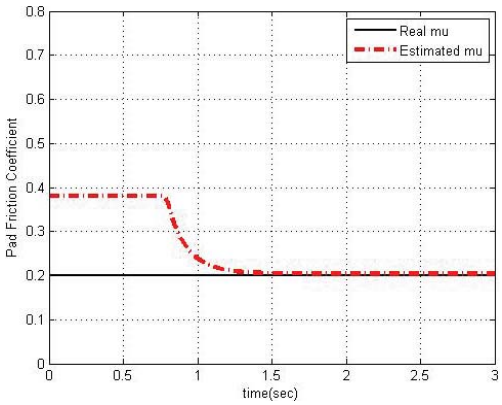

Fig. 13. Adaptation of pad friction coefficient ($\mu_{\text{Plant}} = 0.2$).

When the model is accurate, the tracking control is very good, as shown by the dotted lines in Fig. 9. However, it can be confirmed that the signal fails to track the desired reference when there is parametric uncertainty between the plant and the model. It is confirmed from Fig. 10 that simply increasing control gain K can cause severe chattering problem.

C. Adaptive Control Algorithm Design

To solve the tracking control issue shown in Fig. 10, an adaptive control algorithm is proposed. Stability and convergence performance of the proposed algorithm is proven by using the Lyapunov theory [10]. It should be noted that the control system of the noncircular gear brake is a nonautonomous system.

If the control input induced by using the nominal value of the brake pad friction coefficient is defined as $\hat{u}_M$

$$\hat{u}_M = q^{-1}\Big[\hat{p}_1\theta_M^2 + p_2\omega_M + \dot{\omega}_{Md} - (\lambda + K)(\omega_M - \omega_{Md}) - \lambda K(\theta_M - \theta_{Md})\Big]. \tag{44}$$

If $\hat{u}_M$ is substituted into (41), $\dot{s}$ can be written follows:

$$\begin{aligned}\dot{s} &= -(p_1 - \hat{p}_1)\theta_M^2 - Ks \\ &= n(\mu - \hat{\mu})\theta_M^2 - Ks \\ &\quad \times \left(n = \frac{K_{\text{Cal}}\tan^2\alpha L^3}{J_M(\cos\beta + \tan\alpha\sin\beta)8\pi^3\eta\cos^2\beta}\right). \end{aligned}\tag{45}$$

This paper suggests an adaptive algorithm in the following:

$$\dot{\hat{\mu}} = \frac{n}{\alpha}\theta_M^2 s \tag{46}$$

where, α is a positive constant adaptation gain.

Proposition 1: Consider the dynamic system in (37). If the control input selected according to (44) with the adaptive law (46), then the convergence of the tracking error (38) is guaranteed.

Proof: Equations (45) and (46) represent closed-loop dynamics of the entire system inclusive of the adaptation. s and $\tilde{\mu} = (\mu - \hat{\mu})$ denote the tracking error and parametric error, and can be seen as two states of the closed-loop dynamics. Since θ_M is time-variant, the control system is a nonautonomous. Therefore, the lower bounded Lyapunov function is defined as follows:

$$V = \frac{1}{2}s^2 + \frac{\alpha}{2}\tilde{\mu}^2 > 0. \tag{47}$$

s is the tracking error of the motor position and velocity, and is bound mechanically and physically. $\tilde{\mu}$ is a parametric error of the brake friction coefficient; since it is known that μ has a value between 0.2 and 0.6, $\tilde{\mu}$ is also bound. Differentiating (47)

$$\dot{V} = s \cdot \dot{s} - \alpha\tilde{\mu} \cdot \dot{\hat{\mu}}. \tag{48}$$

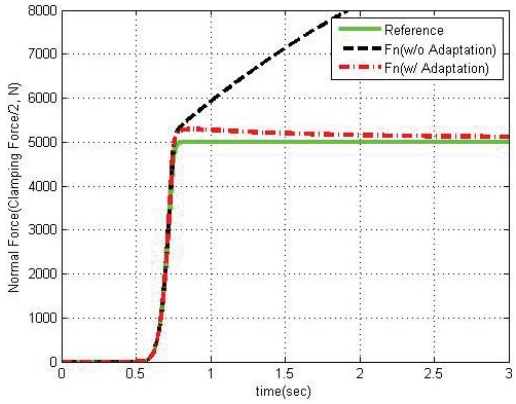

Fig. 14. Adaptive control with $\mu_{\text{Plant}} = 0.6$.

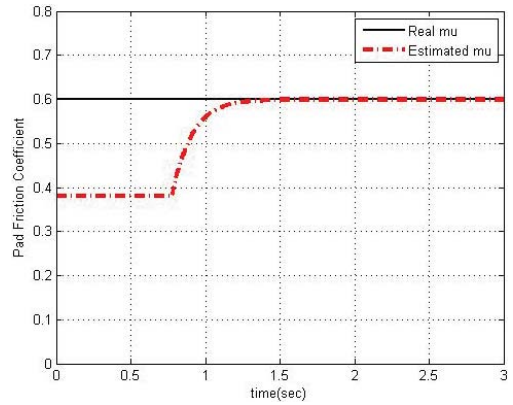

Fig. 15. Adaptation of pad friction coefficient ($\mu_{\text{Plant}} = 0.6$).

Substituting (45) and (46) into (48)

$$\begin{aligned}\dot{V} &= s \cdot \left(n\left(\mu - \hat{\mu}\right)\theta_M^2 - Ks\right) - \alpha\left(\mu - \hat{\mu}\right) \cdot \dot{\hat{\mu}} \\ &= -Ks^2 + \left(\mu - \hat{\mu}\right)\left(n\theta_M^2 s - \alpha \cdot \dot{\hat{\mu}}\right) \\ &= -Ks^2 + \left(\mu - \hat{\mu}\right)\left(n\theta_M^2 s - \alpha \cdot \frac{n}{\alpha}\theta_M^2 s\right) \\ &= -Ks^2 \leq 0. \end{aligned} \tag{49}$$

Convergence of the suggested adaptive algorithm can be proven by using Babalat's lemma [10], [11]. In (49), $\dot{V}$ has a finite limit when $t \to \infty$ since s is upper bounded. $\ddot{V}$ is then calculated to verify the uniform continuity of the differentiable function

$$\ddot{V} = -2Kn\theta_M^2 s\tilde{\mu} + 2K^2 s^2. \tag{50}$$

Since s and $\tilde{\mu}$ are bound, it can be confirmed that $\ddot{V}$ is also bound. Applying Babalat's lemma, $s \to 0$ when $t \to \infty$. From (45), if s converges to 0, $\tilde{\mu}$ converges to 0 under the condition that θ_M is not identically 0.

Fig. 11 schematically illustrates the adaptive control system of the electronic noncircular gear brake. Figs. 12–15 show the simulation results of the developed adaptation controller. The straight lines denote references, dotted lines represent the cases without adaptation, and dashed dot lines represent the cases with adaptation. Figs. 12 and 13 represent the cases when the friction coefficient is at a minimum, while Figs. 14 and 15 represent when it is at a maximum.

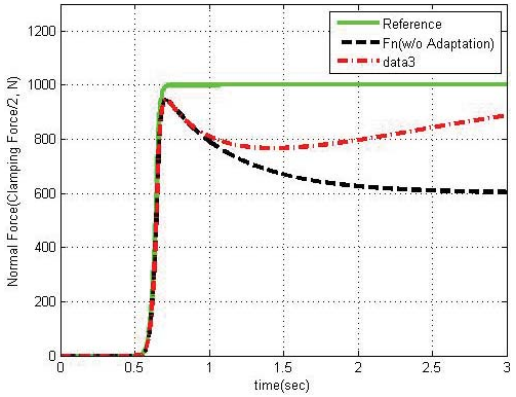

Fig. 16. Adaptive control with small reference input ($\mu_{\text{Plant}} = 0.2$).

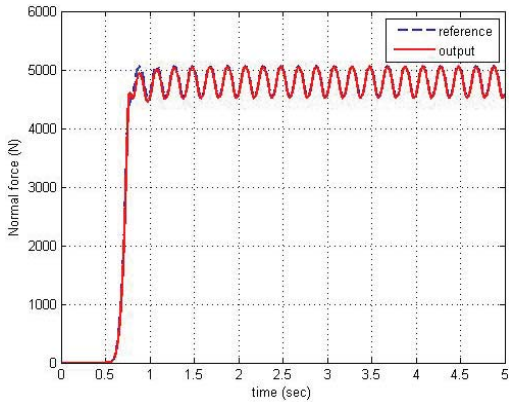

Fig. 17. Adaptive control with sinusoidal reference input ($\mu_{\text{Plant}} = 0.2$).

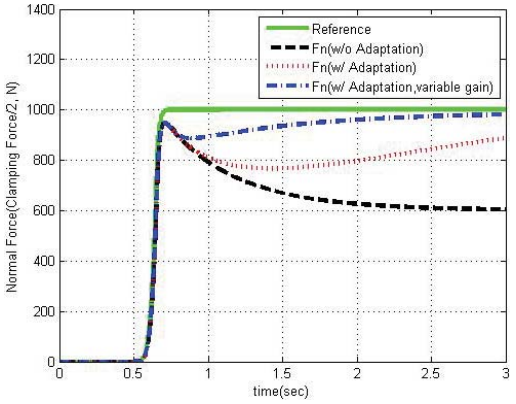

Fig. 18. Modified adaptive control with small reference input ($\mu_{\text{Plant}} = 0.2$).

Fig. 16 represents the reaction of the adaptive controller when the reference input is small. Fig. 17 represents the reaction of the adaptive controller with sinusoidal reference input.

Compared to the previous simulation results, it is confirmed that the tracking velocity decreases drastically. This is due to the fact that adaptation speed of the algorithm described in (46) is proportional to the magnitude of θ_M. To solve this issue, the gain α is redefined as a function of θ_M as follows:

$$\alpha = \alpha_1 + \alpha_2\theta_M^2, \qquad \alpha_1 > 0, \qquad \alpha_2 > 0. \tag{51}$$

The simulation results in Fig. 18 show that the tracking velocity does not slow down with θ_M anymore.

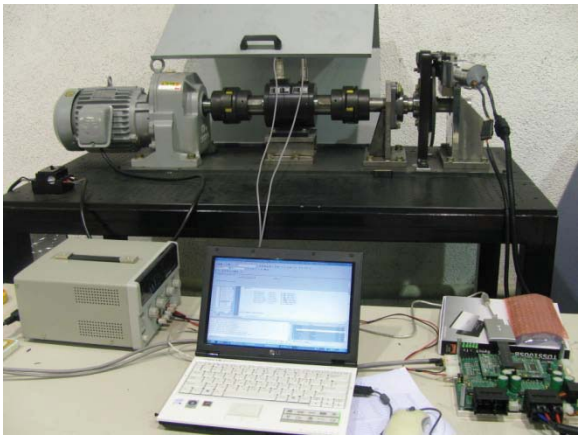

Fig. 19. Test bench.

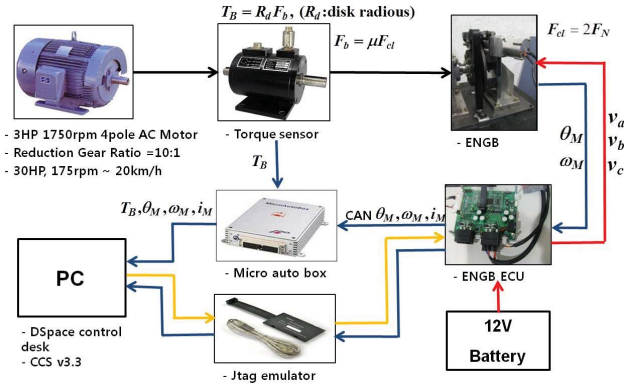

Fig. 20. Test bench control set up.

IV. Experiment

The control algorithm developed in previous section is evaluated experimentally. Fig. 19 shows the actual setup of the test bench. The brake disc is driven by a 2.2 kW three-phase AC motor. The motor torque is amplified by a 10:1 reduction gear, and the disc runs at 176 rpm, or 20 km/h if translated to the vehicle speed. A sensor to measure the brake torque and the rotation speed is located in the middle of the apparatus. The sensor signal is used just for monitoring, and is not used for the real time control.

Fig. 20 shows the control setup of the test bench. The control algorithm written with C Code Composer Studio v3.3 is downloaded onto ECU through a Jtag emulator. The desired normal force value is entered in real time through the Jtag emulator, which converts it to the desired position input at ECU, and receives feedback for position and velocity values through the motor's position sensor to calculate the control input (voltage). The position, velocity, inverter current, and the torque sensor signals are monitored through Micro-Autobox. The processing time of the controller is 1 ms.

A. Experimental Verification of Self-Energizing Effect

First, the self-energizing effect of the electronic non-circular gear system is confirmed through an experiment.

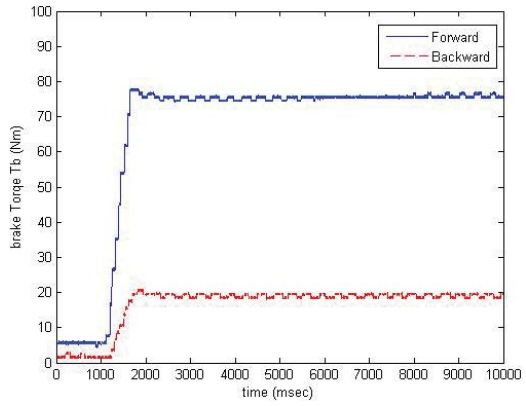

Fig. 21. Brake torque.

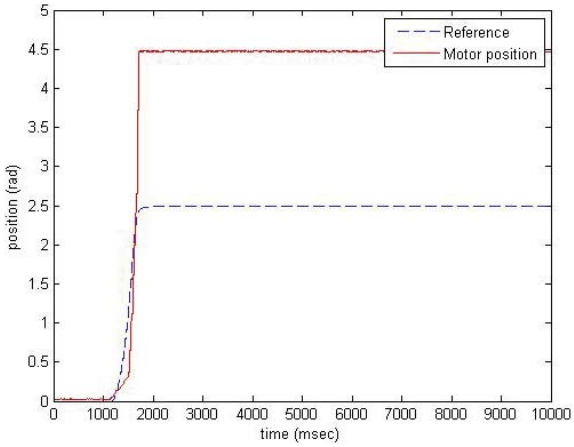

Fig. 22. Without adaptation: reference motor position equivalent to 1000-N brake normal force, $\hat{\mu}_0 = 0.25$.

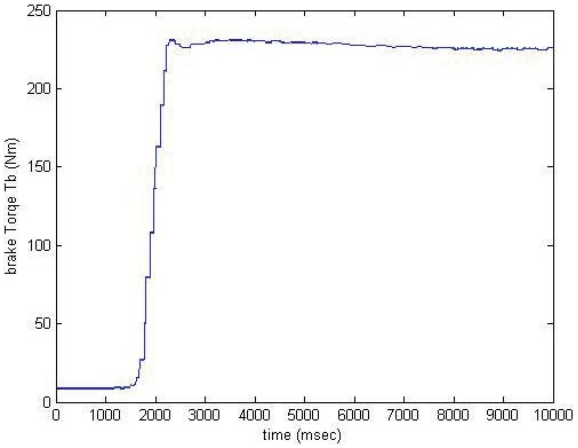

Fig. 23. Without adaptation: brake torque, $\hat{\mu}_0 = 0.25$.

Voltage is applied as a step input, and the brake torque was measured through the torque sensor. Fig. 21 shows the resulting brake torque when the disc is rotated in both directions, while the same amount of voltage input is applied on the motor. From this experiment, it is confirmed that the brake gain increases dramatically due to the self-energizing effect when the disk is rotating in the normal direction.

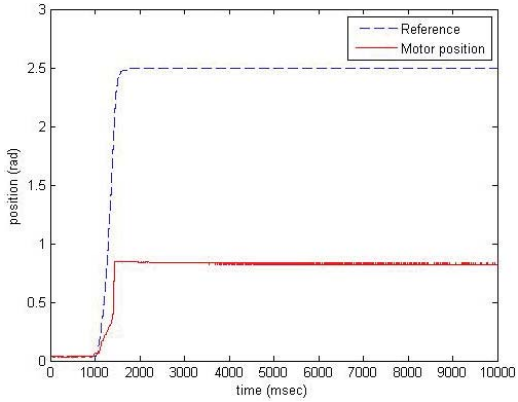

Fig. 24. Without adaptation: reference motor position equivalent to 1000-N brake normal force, $\hat{\mu}_0 = 0.55$.

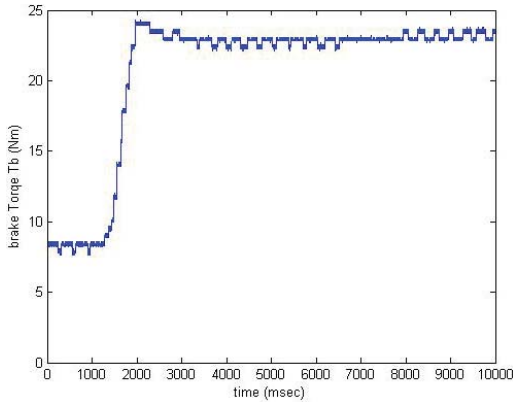

Fig. 25. Without adaptation: brake torque, $\mu_{\text{model}} = 0.55$.

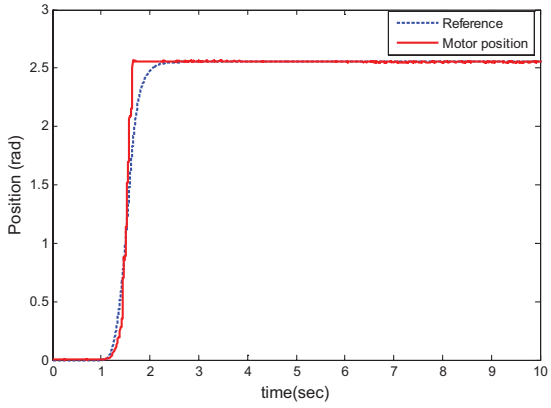

Fig. 26. Adaptive control: reference motor position equivalent to 1000-N brake normal force.

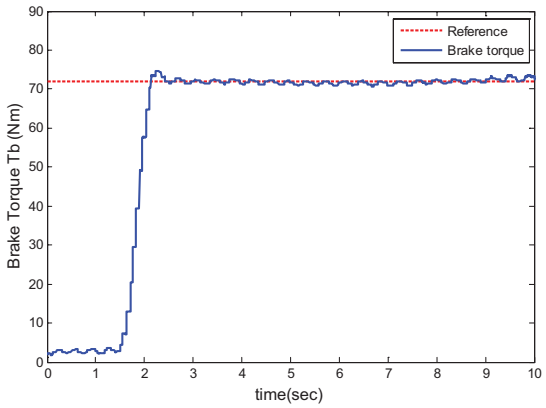

Fig. 27. Adaptive control: brake torque.

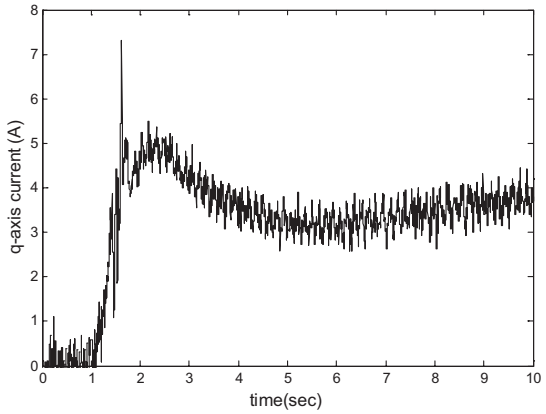

Fig. 28. Adaptive control: motor current.

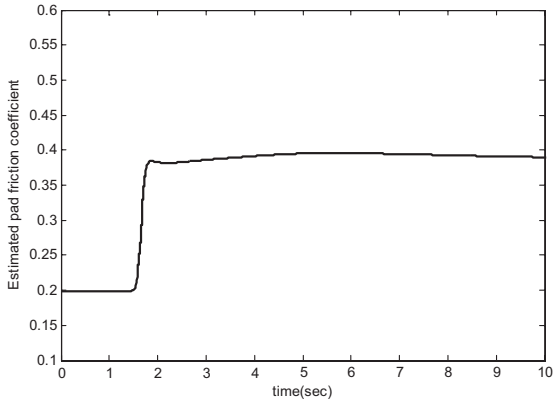

Fig. 29. Adaptive control: estimated μ.

B. Adaptive Sliding Mode Control

In order to compare and validate the performance of the adaptive controller, a pad friction coefficient value different from that of the plant is entered into the model as an initial value for the experiment. Figs. 22–25 show outcomes of the experiment when the adaptive algorithm is not activated. Figs. 22 and 23 show the position tracking performance and brake torque when the model's brake pad friction coefficient value is smaller than that of the plant, while Figs. 24 and 25 show the position tracking performance and brake torque when the model's brake pad friction coefficient value is greater than that of the plant.

Figs. 26–32 show outcomes of the experiment for which the adaptive algorithm is activated. Figs. 26–29 show the motor position tracking performance, brake torque, motor current, and estimated brake pad friction coefficient when the initial value of the estimated friction coefficient is 0.2, which is lower than the actual value. It can be confirmed that the tracking performance improves greatly compared to the case without adaptation.

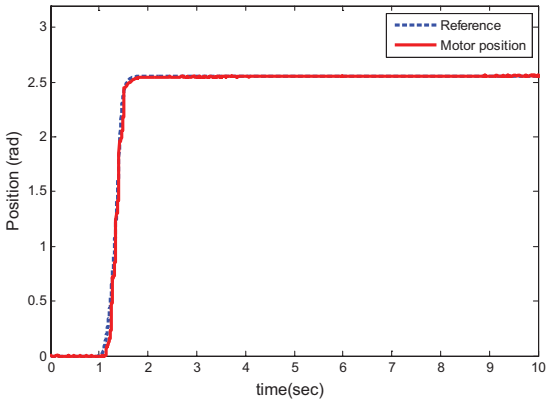

Fig. 30. Adaptive control: reference motor position equivalent to 1000-N brake normal force.

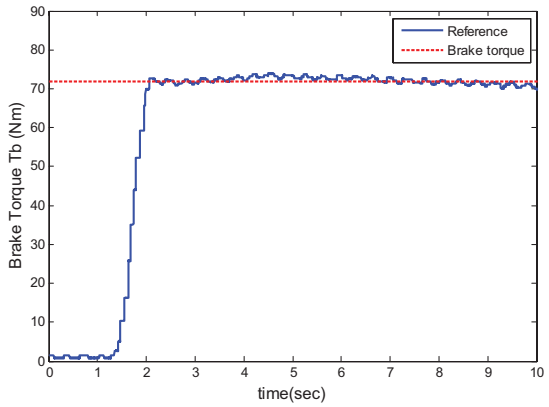

Fig. 31. Adaptive control: brake torque.

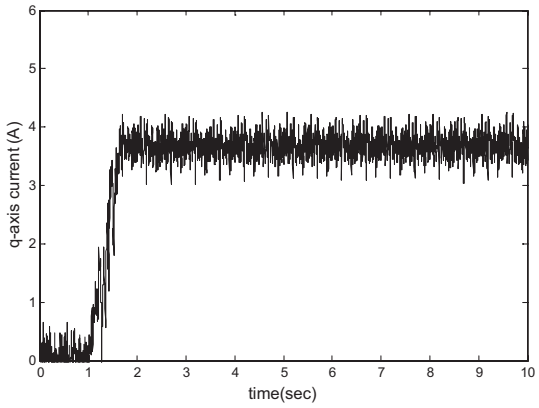

Fig. 32. Adaptive control: motor current.

Figs. 30–32 show the motor position tracking performance, brake torque, and motor current. Estimated brake pad friction coefficient when the initial value of the estimated friction coefficient is 0.38, which is same as the plant value.

V. Conclusion

In this paper, kinetic and dynamic characteristics of a newly designed noncircular gear were analyzed. The nonlinearity of the caliper stiffness was modeled and applied to the clamping force control. A fifth-order model that takes angular position and speed of a noncircular gear; angular position, and speed of the motor; and electric current as its states was developed. For the model-based controller design, model reduction was performed by using a singular perturbational method. Based on the obtained reduced-order model, a pseudo-sliding controller that does not require a clamping force sensor was designed.

Simulation results revealed that the tracking performance deteriorates significantly depending on the changes of pad friction coefficient. Therefore, an adaptive controller was developed and validated through simulations and experiments. Experimental results showed that the actually working brake torque on the disc was amplified significantly due to self-energizing effect. When the proposed adaptive control algorithm was applied, it was confirmed that the tracking performance improved dramatically compared to the cases without parameter adaptation.

References

[1] H. Hartmann, M. Schautt, A. Pascucci, and B. Gombert, "eBrake - the mechatronic wedge brake," SAE, Warrendale, PA, Tech. Rep. 2002-01-2582, 2002.

[2] R. Roberts, M. Schautt, H. Hartmann, and B. Gombert, "Modeling and validation of the mechatronic wedge brake," SAE, Warrendale, PA, Tech. Rep. 2003-01-3331, 2003.

[3] R. Roberts, B. Gombert, H. Hartmann, D. Lange, and M. Schautt, "Testing the mechatronic wedge brake," SAE, Warrendale, PA, Tech. Rep. 2004-01-2766, 2004.

[4] Á. Semsey and R. Roberts, "Simulation in the development of the electronic wedge brake," SAE, Warrendale, PA, Tech. Rep. 2006-01-0298, 2006.

[5] E. H. Miller, "A note on reflector arrays," *IEEE Trans. Ant. Propag.*, vol. 15, no. 5, pp. 692–693, Sep. 1967.

[6] L. M. Ho, R. Roberts, H. Hartmann, and B. Gombert, "The electronic wedge brake - EWB," SAE, Warrendale, PA, Tech. Rep. 2006-01-3196, 2006.

[7] Y. Hwang and S. Choi, "Adaptive sliding-mode control of electronic wedge brake," KSAE, Seoul, Korea, Tech. Rep. 1020-1026, 2007.

[8] S. Kim, S. Choi, and J. Kim, "The design of a self-energizing brake system using non-circular gear," KSAE, Seoul, Korea, Tech. Rep. 1793-1801, 2008.

[9] P. Pillay and R. Krishnan, "Modeling, simulation, and analysis of permanent-magnet motor drives. I. The permanent-magnet synchronous motor drive," *IEEE Trans. Ind. Appl.*, vol. 25, no. 2, pp. 265–273, Mar.–Apr. 1989.

[10] J.-J. E. Slotine and W. Li, *Applied Nonlinear Control*. Englewood Cliffs, NJ: Prentice-Hall, 1990.

[11] P. Ioannou and B. Fidan, *Adaptive Control Tutorial*. Philadelphia, PA: SIAM, 2006.

[12] W. Lu, "Modeling and control of switched reluctance machines for electro mechanical brake systems," M.S. thesis, Dept. Electr. Eng., Ohio State Univ., Columbus, 2005.

[13] F. L. Litvin, *Gear Geometry and Applied Theory*. Englewood Cliffs, NJ: Prentice-Hall, 1994.

[14] C. Lee, C. Manzie, and C. Line, "Explicit nonlinear MPC of an automotive electromechanical brake," in *Proc. 17th World Congr. Int. Federat. Autom. Control*, Jul. 2008, pp. 10758–10763.

[15] B. A. Heloutr, P. Dupont, and C. C. De Wit, *A Survey of Models, Analysis Tools and Compensation Methods for the Control of Machines with Friction*. Amsterdam, The Netherlands: Elsevier, 1994.

[16] C. Huang and L. Fu, "Adaptive control approach for speed motion-sensorless of linear induction motor unknown resistance and payload," in *Proc. 17th World Congr. Int. Federat. Autom. Control*, Jul. 2008, pp. 13253–13258.

[17] P. Sicard, K. Al-Haddad, and Y. Dube, "DC motor control using sliding mode and disturbance estimator," in *Proc. 20th Annu. IEEE Power Electron. Special. Conf.*, Jun. 1989, pp. 431–437.

[18] H. A. F. Mohamed, S. S. Yang, and M. Moghavvemi, "Integral sliding mode control for improved robustness and accuracy of induction motors," in *Proc. 17th World Congr. Int. Federat. Autom. Control*, Jul. 2008, pp. 6283–6288.

[19] J.-J. E. Slotine and J. A. Coetsee, "Adaptive sliding controller synthesis for non-linear systems," *Int. J. Control*, vol. 43, no. 6, pp. 1631–1651, 1986.
[20] N. S. Nise, *Control Systems Engineering*. New York: Wiley, 2004.
[21] H. K. Khalil, *Nonlinear Systems*. Englewood Cliffs, NJ: Prentice-Hall, 2002.
[22] V. I. Utkin, "Variable structure systems with sliding modes," *IEEE Trans. Autom. Control*, vol. 22, no. 2, pp. 212–222, Apr. 1977.
[23] J. Yi, L. Alvarez, and R. Horowitz, "Adaptive emergency braking control with underestimation of friction coefficient," *IEEE Trans. Control Syst. Technol.*, vol. 10, no. 3, pp. 381–392, May 2002.
[24] R. Rajamani, *Vehicle Dynamics and Control*. New York: Springer-Verlag, 2005.
[25] K. V. Fernando and H. Nicholson, "Singular perturbational model reduction in the frequency domain," *IEEE Trans. Autom. Control*, vol. 27, no. 4, pp. 969–970, Aug. 1982.

Heeram Park received the B.S. degree in mechanical engineering from Handong University, Pohang, Korea, in 2008, and the M.S. degree in mechanical engineering from the Korea Advanced Institute of Science and Technology, Daejeon, Korea, where he is currently pursuing the Ph.D. degree in mechanical engineering.

His current research interests include automotive systems, nonlinear control, and integrated design and control of complex mechanical systems.

Seibum B. Choi received the B.S. degree in mechanical engineering from Seoul National University, Seoul, Korea, in 1985, the M.S. degree in mechanical engineering from the Korea Advanced Institute of Science and Technology (KAIST), Daejeon, Korea, in 1987, and the Ph.D. degree in controls from the University of California, Berkeley, in 1993.

Since 2006, he has been with the Faculty of the Mechanical Engineering Department, KAIST. He was engaged in the development of automated vehicle control systems with the Institute of Transportation Studies, University of California, from 1993 to 1997. In 2006, he was with TRW Automotive, Livonia, MI, where he was engaged in the development of advanced vehicle control systems. His current research interests include fuel-saving technology, vehicle dynamics and control, and active safety systems.